© Copyright 2024

Qizheng Yang

Designed Peptoid-Based Metal-Containing Nanosheets as Enzyme Mimetics for Catalytic CO2 hydration

Qizheng Yang

A thesis

submitted in partial fulfillment of the

requirements for the degree of

Master of Science in Applied Chemical Science and Technology

University of Washington

2024

Committee:

Chun-Long Chen

Brandi M. Cossairt

Program Authorized to Offer Degree:

Chemistry

University of Washington

Abstract

Designed Peptoid-Based Metal-Containing Nanosheets as Enzyme Mimetics for Catalytic CO2 Hydration

Qizheng Yang

Chair of the Supervisory Committee:

Chun-Long Chen

Department of Chemistry

The continued rise in CO2 levels worldwide has attracted widespread concern among researchers. Carbonic anhydrase, a carbon dioxide hydratase widely found in nature, has extremely high catalytic activity in CO2 hydration. However, because it is difficult to extract and preserve and is easily inactivated, much effort has been put into artificially synthesizing it. Herein, we developed a series of peptoid-based metal-containing nanosheets with natural carbonic anhydrase-like activities. We tested their catalytic activities under different conditions. The results

showed that some of them have good catalytic activity and are promising candidates for artificial carbonic anhydrase mimics.

INTRODUCTION

1.1 Global Warming and Its Solutions

With the development of modern society, humanity's demand for fossil fuels is unprecedented. As one of the main combustion products of fossil fuels and the main cause of the greenhouse effect, excessive emissions of carbon dioxide have become a serious problem worldwide. It is predicted that carbon dioxide emissions will be 30%-50% higher than in 1990 in 60 years.[1] Many solutions have been proposed to slow down global warming. The main ideas of most of the solutions are either limit the usage of fossil fuels or replace fossil fuels with renewable energy. However, power generation based on fossil fuels is still needed to meet the massive energy demands.[2] [3]. Therefore, the most reliable way to deal with excessive CO_2 for now is Carbon Capture, Utilization, and Storage, which is called CCUS. The first step, carbon capture, can be achieved in many ways, as shown in Figure 1-1[4]. In this thesis, we pay our attention on a simple reaction, which is CO_2 hydration ($CO_2 + H_2O \rightleftharpoons HCO_{3-} + H^+$). This reaction is of great importance when capturing CO_2 in an aqueous system.[6]

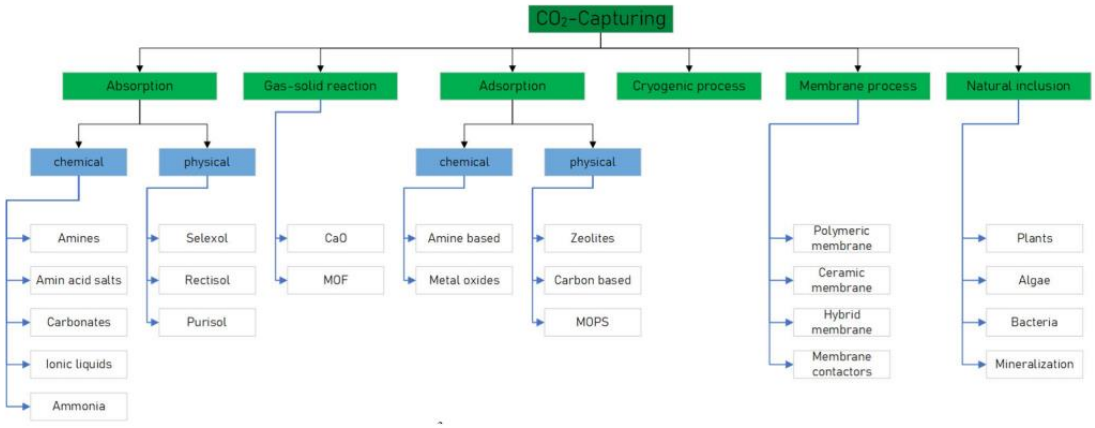

Figure 1-1 CO_2-Capturing pathways [4]

1.2 Carbonic Anhydrase (CA) and CA Mimics for CO_2 Hydration

Although CO_2 hydration can occur in uncatalyzed conditions. However, it is highly pH dependent and very slow in acidic or neutral conditions. Catalysts can significantly accelerate CO_2 hydration and it can be achieved by biocatalysis, biomimetic homogeneous catalysis and biomimetic heterogeneous catalysis. These pathways will be discussed below.

1.2.1 Biocatalytic CO_2 Hydration

Carbonic anhydrase (CA) has been reported as the most effective enzyme for CO_2 hydration. CA is a crucial enzyme found in many living organisms. All animals, some of the organisms that need photosynthesis, and some bacteria contain CAs [5]. There are six species of CAs coming from different organisms that have been reported, which can be categorized to the α-, β-, γ-, δ-, ζ- and η- CAs [7]. CAs are metalloenzymes with metal-containing active sites and only have

catalytic activity with the metal cation inside. Most species of CAs contain Zn (II), while some species of CAs may contain Fe (II) or Cd (II). Zn (II) of some types of α-CA can be replaced by Co (II) and can still maintain much of the catalytic activity. [3][7] Their coordination patterns are shown in Figure 1-2(a)-(e).

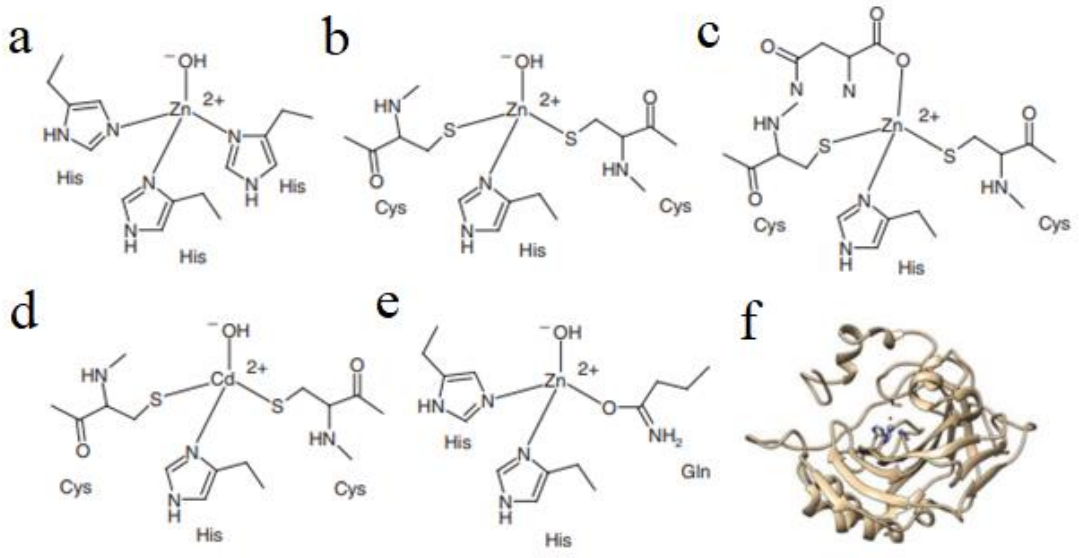

Figure 1-2 [7]

Human CA II, which belongs to α-CA, has one of the highest catalytic activities among any other species of CAs. Its structure is shown in Figure 1-2(f).

The mechanism of Human CA II catalyzed CO2 hydration includes several steps: (Figure 1-3)

Step1: Water molecule is absorbed and form a Zn (II)- hydroxide ion complex. Step2: Nucleophilic attack of oxygen atom from Zn (II)-hydroxide ion complex on the carbon atom of CO_2. Step3: The formation

of bicarbonate intermediate. Step4: Rearrangement of proton on bicarbonate ion. Step5: Exchange of rearranged bicarbonate ion and water, a cycle is completed. [3][8]

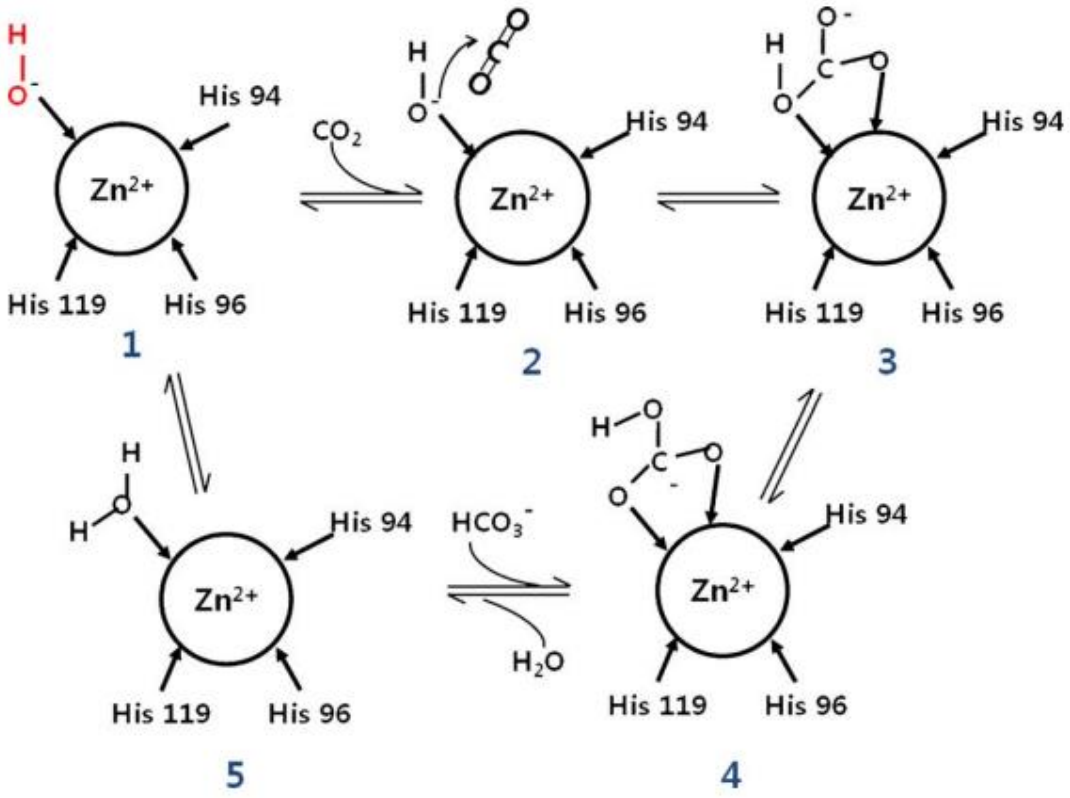

Figure 1-3 [8]

Proton transfer with the help of histidine residues is the rate-limiting step. Therefore, a base or buffer condition is needed to deprotonate the histidine residues. [9]

Although Human CA II has the highest catalytic activity, it is impossible to extract and utilize large amounts of CA II from the human body. Therefore, researchers have put much effort into extracting CA from different organisms like plants and bacteria. Even so, it is difficult for natural enzymes to meet industrial needs due to the high extraction cost

and these natural enzymes are difficult to store, and they are also sensitive to temperature. Their catalytic activity varies a lot with the temperature. And they are most likely to lose catalytic activity under industrial absorbance temperatures (40-60 °C). Therefore, it is crucial to develop catalysts that are easy for massive production and have high catalytic activity and thermal stability.

1.2.2 Biomimetic Homogeneous Catalytic CO_2 Hydration

Over the years, researchers have developed many metal-ligand complexes to mimic natural CAs. The main ideas of the design of these metal-ligand complexes are to mimic the active site of CA.[11] As previously introduced, in CA's active site, a Zn (II) coordinates with the nitrogen atoms of three histidine and the oxygen atom of a hydroxide ion. Based on this structure, many metal-ligand complexes, like Zinc Cyclen (1,4,7,10-tetraazacyclodo-decane zinc complex) and Zn-tri (1,5,9-triazacyclododecane zinc complex) have been designed. As mentioned earlier, Zn (II) of some types of CA can be replaced by Co (II) and can still maintain much of the catalytic activity. Therefore, other metal-ligand complexes containing Co (II) like Co-BBP (2,6-bis(2-benzimidazolyl)pyridine cobalt complex) or C1P (1-(3-formyl-4-hydroxybenzyl)-3-triphenylphosphonium-salen(P)-Co$(NH_3)_2$]Cl_3).

Besides them, there are a lot of different designs. Their structures are shown in Figure 1-4. Some other transition metals like Ni and Cu have

also been used to construct metal-ligand complexes that mimic CA.

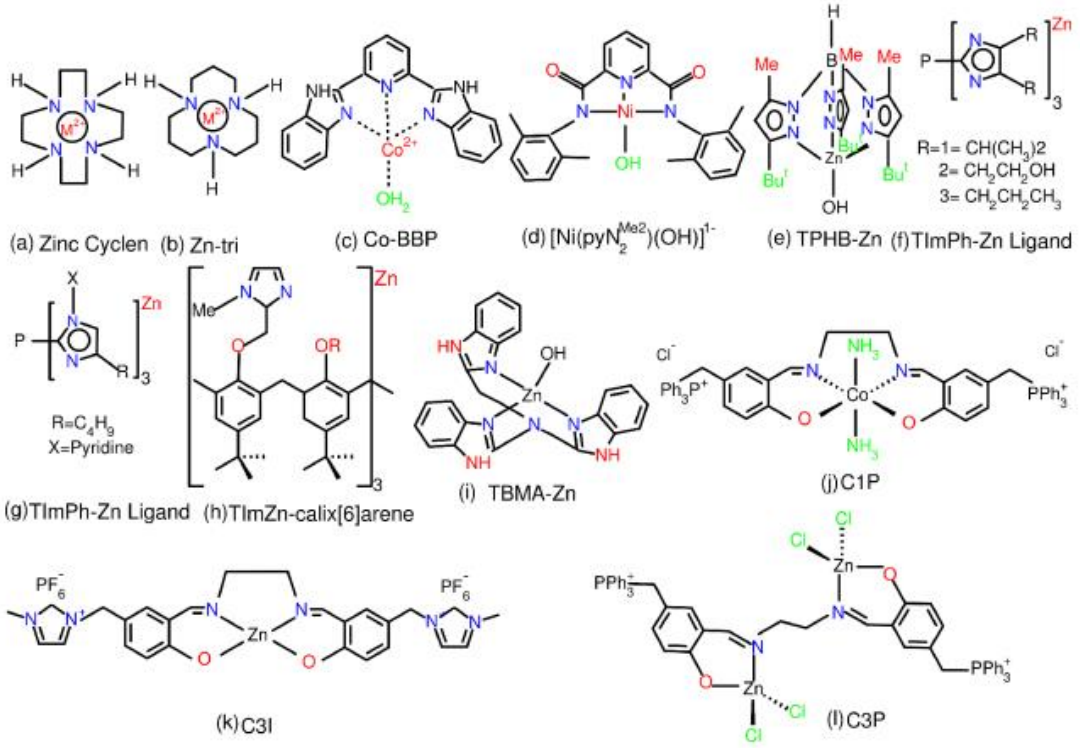

Figure 1-4 [3]

CA mimic organometallic molecules for CO_2 hydration: (a) 1,4,7,10-tetraazacyclodo-decane zinc complex, (b) 1,5,9-triazacyclodo-decane zinc complex, (c) 2,6-bis(2-benzimidazolyl)pyridine cobalt complex, (d) N,N′-2,6-dimethylphenyl-2,6-pyridinedicarbo-amidate dianion nickel complex, (e) tris(pyrozolyl)hydroborate, (f,g) tris(imidazolyl)-phosphine zinc complex, (h) tris(imidazolyl) zinc calix[6]arene, (i) tris(2-benzimidazolmethyl)amine zinc complex, (j) 1-(3-formyl-4-hydroxybenzyl)-3-triphenylphosphonium-salen(P)-Co$(NH_3)_2$]Cl_3, (k) 1-(3-formyl-4-hydroxybenzyl)-3-triphenylphosphonium-salen(I)−Zn-hexafluorophosphate complex, and (l) Zn(1-(3-formyl-4-hydroxybenzyl)-3-triphenyl-phosphonium-salen(P)Cl_4.

One of the most well studied metal-ligand complexes CA mimic is zinc cyclen. Zinc ion in zinc cyclen will coordinate with a water molecule in solvent. Its catalytic mechanism for CO_2 hydration is similar to CA. Comparing to CA, although the CO_2 hydration kinetics of zinc cyclen is much slower[12], the molecular weight of zinc cyclen is also much lower. As a result, the catalytic activities of natural CA and zinc cyclen are of

the same order of magnitude when they are in the same mass, zinc cyclen is only 5 times slower than natural CA. This makes zinc cyclen possible for industrial utilization. Furthermore, experiments have proved that zinc cyclen will not only maintain catalytic activity and its structure in high temperatures, but its catalytic activity can increase with the temperature. [13] This makes zinc cyclen a promising catalyst for CO_2 hydration in industrial conditions.

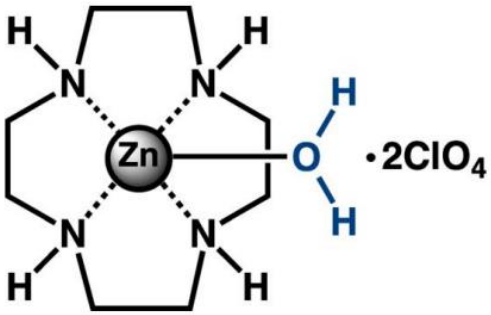

Figure 1-5 Zinc cyclen perchlorate

1.2.3 Biomimetic Heterogeneous Catalytic CO_2 Hydration

Although these zinc cyclen like metal-ligand CA mimics have many advantages in industrial operations. However, using these catalysts for homogeneous catalysis makes them hard to recycle. Therefore, for these catalysts to be easier to recycle, they need to be immobilized. There are several methods to immobilize CA mimic for industrial utilization such as adsorption, covalent bonding and crosslinking, encapsulation, and entrapment. Although immobilization will lose some of the activity, the reusability is significantly increased.[1] Thus, immobilized CA mimics are ideal catalysts for industrial CO_2 hydration.

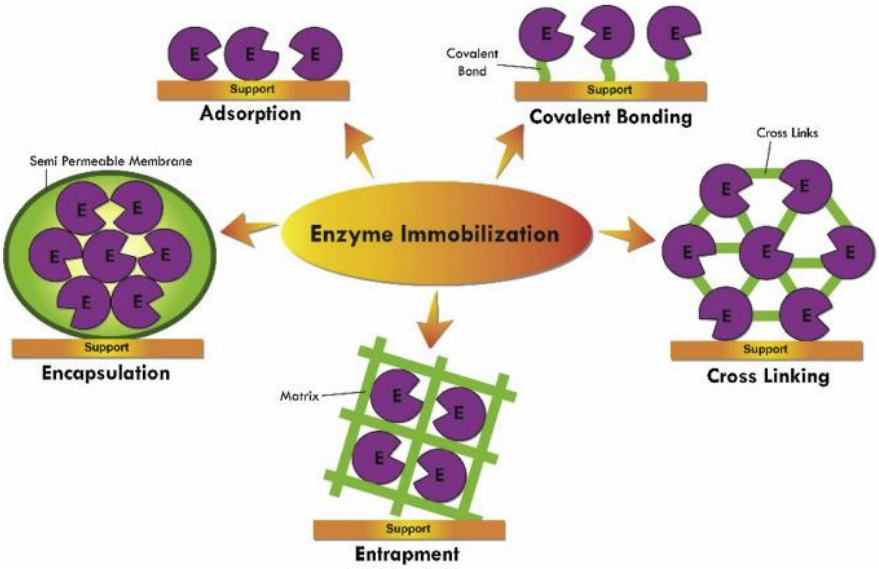

Figure 1-6 Enzyme immobilization methods

1.3 Peptoid

1.3.1 Structure and Self Assembly of Peptoids

Peptoids, also known as poly-N-substituted glycines, are a class of peptidomimetics in which the side chains are attached to the nitrogen atom of the peptide backbone, rather than the alpha-carbon as in natural α-peptides. The comparison of the structure of α-peptide and peptoid is shown in Figure 1-7.

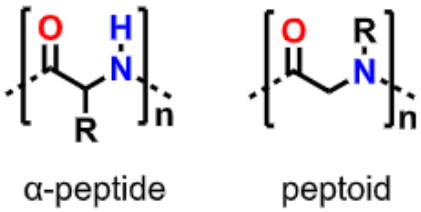

Figure 1-7 α-peptide vs. peptoid

This structural modification provides peptoids with unique properties compared to traditional peptides. Due to the lack of intermolecular

hydrogen bonding interactions and chirality, it is easier to control the secondary and/or tertiary structures of peptoid self-assemblies by simply modifying the side chains. Through wisely design of peptoid monomer it can self-assemble to various morphology such as nanosheets, nanoribbons, helices, vesicles, etc.[10][14]

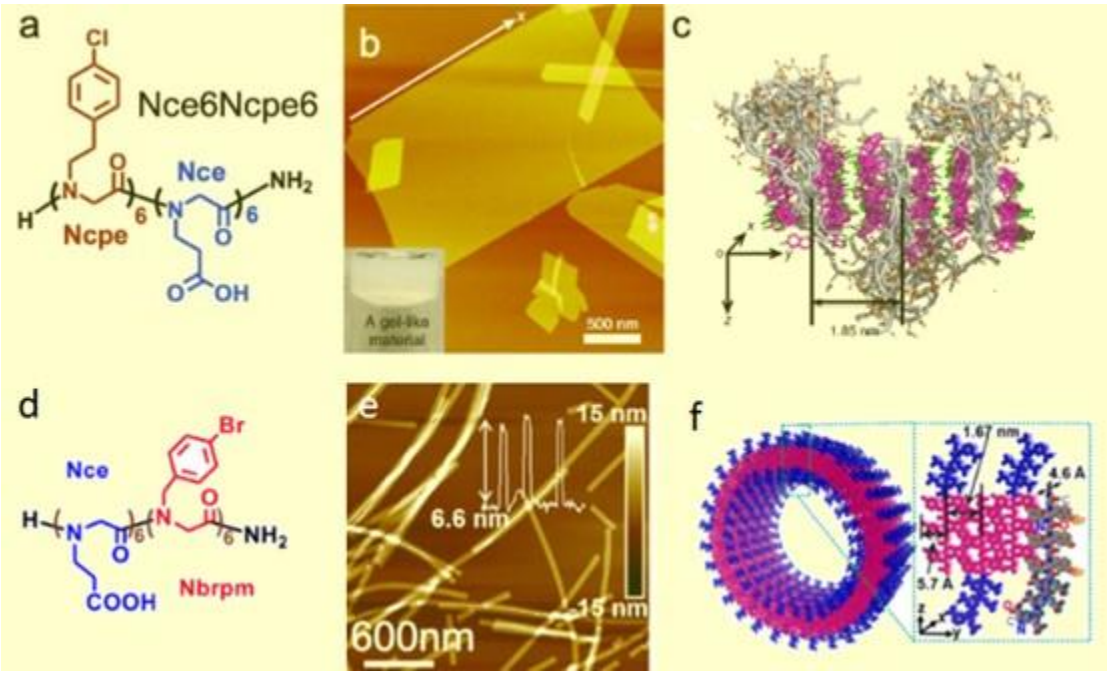

Figure 1-8 (a) Molecular structure of nanosheet forming peptoid Nce6Ncpe6. (b) AFM image of Nce6Ncpe6 peptoid nanosheets. (c) Proposed packing model of Nce6Ncpe6 nanosheets (d) Molecular structure of nanotube forming peptoid d Nbrpm6Nce6. (e) AFM image of Nbrpm6Nce6 peptoid nanotubes. (f) Model of molecular packing of the peptoid nanotube

As we can see in Figure 1-8, these two peptoids have the same hydrophilic domain Nce6 but different hydrophobic domain: Nbrpm6 and Ncpe6 and they self-assemble into different morphology. This indicates that the property of hydrophobic domain is one factor that affects the morphology of peptoid self-assemblies. Furthermore, other factors such as pH, temperature, and solvent may also affect the

morphology.[15][16][17][18]

1.3.2 Peptoid synthesis

Peptoid can be synthesized using solid phase submonomer synthesis. The reaction starts from resin-bound amine. In the first step, the acylation reaction occurs when halo-acetic acid is introduced. In the second step, by nucleophilic attack of primary amine with specific functional group, the growth of carbon chains and the introduction of side chains are successfully achieved. This cycle can be repeated using the produced secondary amine. The final peptoid will be cut off from the resin when all the reactions are completed.

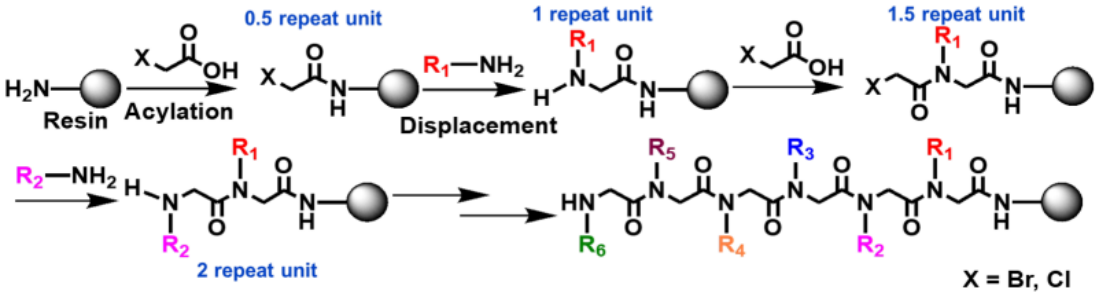

Figure 1-9 Submonomer synthesis of peptoid

1.3.3 Peptoid Assemblies as Enzyme Mimetics

Peptoid is a promising platform to build biomimetic materials. Kim et al reported an antibody mimetic constructed from peptoid nanosheet. They used the automated solid phase submonomer synthesis method to obtain a library of individual loopoid strands. These loopoid strands were then used for supramolecular assembly. Then the Förster resonance energy

transfer is used to test the binding affinity of the assembled loopoid strands with target proteins. The results showed that peptoid sequences have high binding specificity with anthrax protective antigen. Moreover, due to the chemical properties of the peptoid, these nanosheets were resistant to proteolytic degradation. Proved that biomimetic materials made by peptoid could be not only specific but also stable.[19][20]

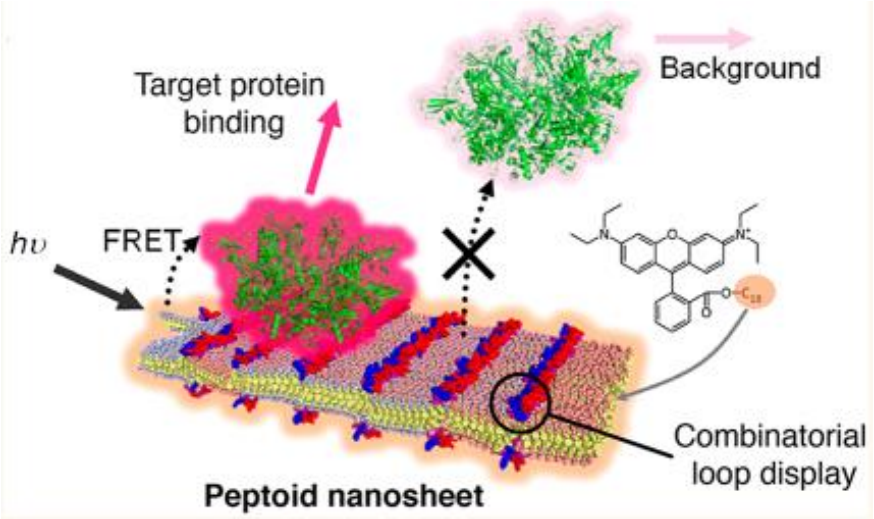

Figure 1-10 Peptoid Nanosheet Antibody Mimetic

Jian et al. reported a series of peptoid/hemin enzymatic mimetics with natural peroxidase-like activities. These enzymatic mimetics exhibited high performance in lignin depolymerization, which is crucial in many industrial processes. The peptoids used to build the enzymatic mimetics mainly consist of two parts: the structure-defining domain, which includes several hydrophilic and hydrophobic groups responsible for forming nanotubes, and the terminal binding domain with coordination sites such as [2-(4-imidazolyl)ethylamine]glycine, [2-(4-pyridyl)ethylamine]glycine, or N-[2-(1H-indol-3-yl)ethyl]glycine that can

bind with hemin to mimic the active site of natural peroxidase. These peptoid/hemin enzymatic mimetics had decent catalytic activities and were more stable and easier to produce compared to natural peroxidase.

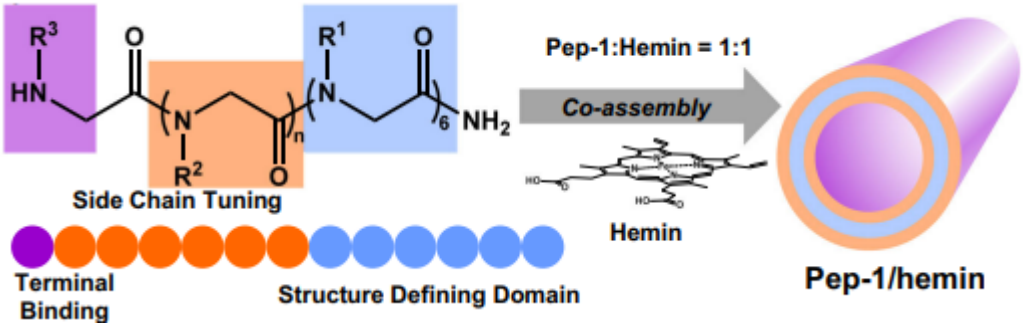

Figure 1-11 Peptoid/Hemin Enzymatic Mimetics

Trinh et al developed a series of metal-containing peptoid membranes that mimic natural enzyme pseudomonas diminuta phosphotriesterase (PTE). PTE is the most efficient enzyme for toxic organophosphates degradation. But it is difficult in extraction or preparation. Moreover, as a natural enzyme, PTE enzyme is easily denatured, which makes it hard to store. To solve this problem, Trinh et al introduced small-molecule metal-binding ligands that mimic the active site of PTE into sequence-defined peptoids and used these peptoids to build membranes by self-assembly. These peptoid membranes were proved to have high catalytic activity for OP degradation and they were resistant to extreme pH, temperature and not easy to dissolve in solvents.

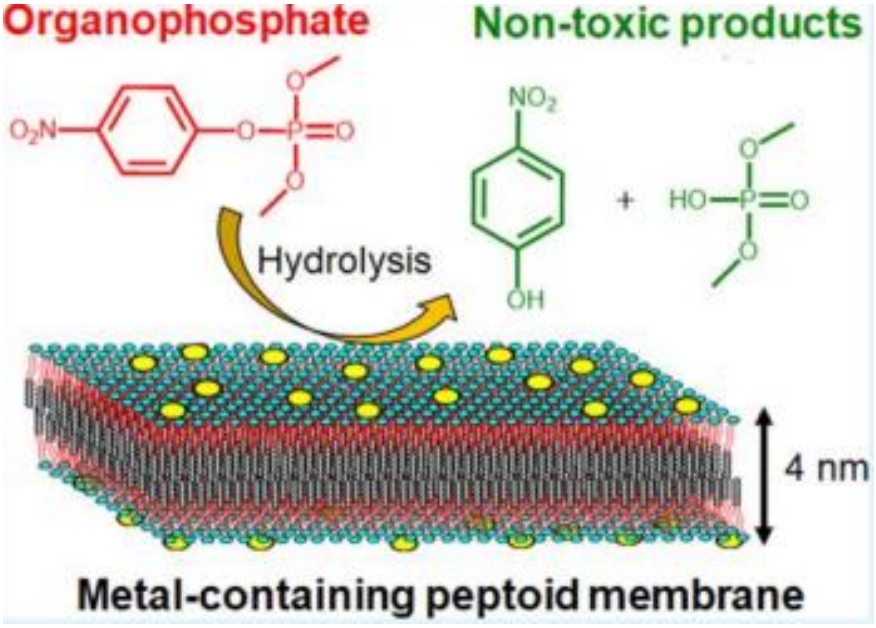

Figure 1-12 Metal-containing peptoid membrane for OP degradation

The above research indicates that peptoid is a powerful tool to build biomimetic materials acting as enzyme mimics. Compared to natural ones, peptoid-based materials are low cost, easy to prepare and have decent stability. Inspired by the above research, we consider using peptoid to build CA mimic. As discussed in 1.2, biomimetic heterogeneous catalysis is a favorable way for industrial CO_2 hydration, and peptoid is an ideal platform to build biomimetic heterogeneous catalyst. This research will exhibit and discuss the recent advances in using peptoid self-assemblies to build CA mimics and assess their catalytic ability by performing p-NPA hydrolysis experiment.

1.4 CA Activity Assay

There are three main CA activity assay methods which are manometric, electrometric, and colorimetric.[1] These methods will be discussed below.

1.4.1 Manometric Assay

Manometric assay is a classic method for CA activity measurement. This method was reported by F J Roughton and V H Booth in 1946 and it was modified by Ralph Karler and Dixon M. Woodbury in 1963. This method directly measures the absorbance of CO_2 by manometer to determine the activity of CA. CO_2 is generated by KH_2PO_4 and sodium bicarbonate stock solution. By measuring the pressure and reaction time, the activity of CA can be calculated. The structure of the device is shown in Figure 1-13. Although this method provides direct physical measurement of reaction dynamics, it is a bit older and less commonly used compared to electrometric and colorimetric methods.

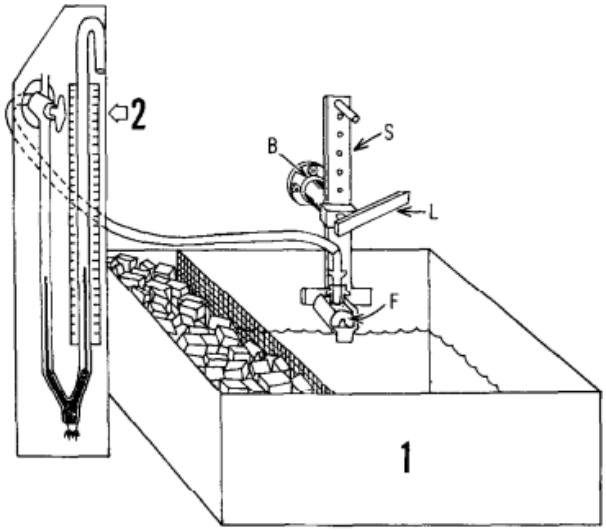

Figure 1-13 Apparatus for manometric determination of carbonic anhydrase

1.4.2 Electrometric Assay

Electrometric assay is reported by Wilbur and Anderson in 1948, so it is

also known as Wilbur and Anderson assay (WAU). This method is based on pH measurements by pH meter. When CO_2 is converted to bicarbonate by CA, the pH will drop. By measuring the end point of pH change, which is around 6.3[21], the reaction rate can be calculated by the formula. The Wilbur and Anderson assay remains a classic method in enzymology for studying carbonic anhydrase and other similar enzymes, providing valuable insights into enzyme mechanism and activity under various experimental conditions. The apparatus of this method is shown in Figure 1-14.

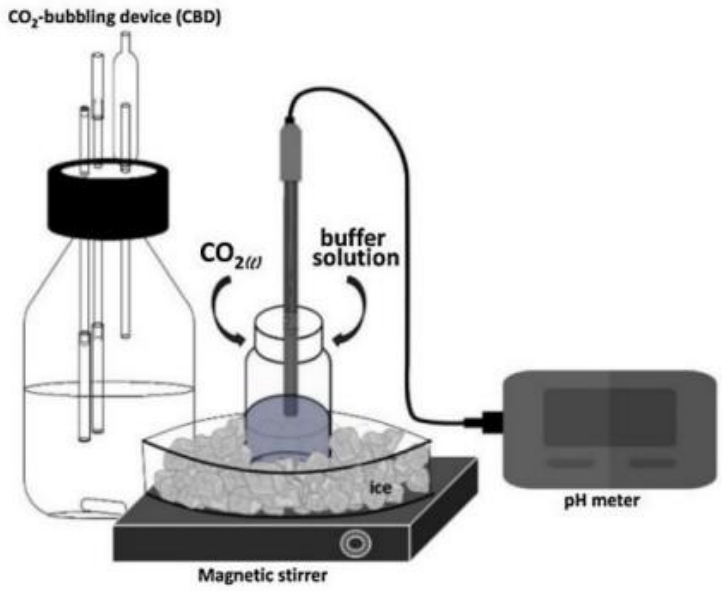

Figure 1-14 Apparatus for electrometric determination of carbonic anhydrase

1.4.3 Colorimetric Assay

The Nitrophenol Acetate (NPA) assay is a widely used method to determine the esterase activity of enzymes, including carbonic anhydrase. This is because besides catalytic activity for CO_2 hydration, CA also has

catalytic hydrolysis activity of esters.[22] [23] [24] This assay is based on the enzymatic hydrolysis of p-nitrophenol acetate to p-nitrophenol and acetate. P-nitrophenol is a chromogenic compound, which makes this reaction particularly useful for spectrophotometric analysis. With the progression of the reaction, the absorbance at the specific wavelength (around 402nm) will increase, the activity of CA can thus be calculated. The NPA assay can be used as a simple preliminary method to test the activity of CA. The apparatus of this method is shown in Figure 1-15.

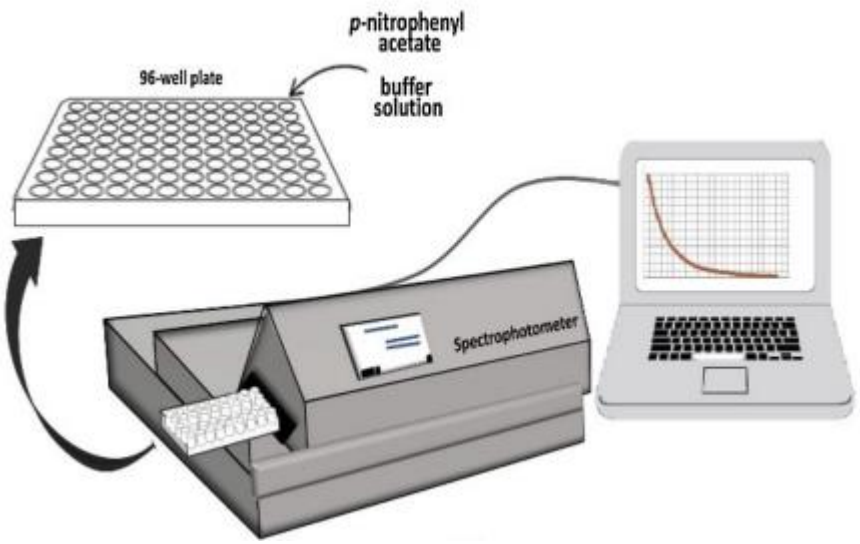

Figure 1-15 Apparatus for colorimetric determination of carbonic anhydrase

MATERIALS AND METHOD

2.1 Materials

All solvents were brought from Fisher or VWR and used without further purification. Bromoacetic acids were purchased from Chem-Impex International, Inc. Rink amide AM resin was purchased from Supra

Sciences. N,N'-diisopropylcarbodiimide (DIC), 4-methylpiperidine (PIP), trifluoroactic acid (TFA), 4-bromophenethylamine (Nbrpe), 4-bromobenzylamine (Nbrpm), tert-butyl N-(2-aminoethyl)carbamate (Nae), β-alanine tert-butyl ester hydrochloride (Nce) were purchased from Oakwood Chemical. Diglycolic anhydride (Dig) was purchased from TCI Chemicals. Fmoc-Gly-OH (Nc2), Fmoc-b-Ala-OH (Nc3) were purchased from Aapptec. 4-nitrophenol (p-NP), 4-nitrophenyl acetate (p-NPA), dichloromethane (DCM), dimethylformamide (DMF), 4-(2-hydroxyethyl)-1-piperazineethanesulfonic acid (HEPES), LC/MS graded acetonitrile (ACN), Zinc tetrafluoroborate hydrate ($Zn(BF_4)_2$), Copper tetrafluoroborate hydrate ($Co(BF_4)_2$), and copper(II) tetrafluoroborate hexahydrate ($Cu(BF_4)_2$) were brought from Thermo Scientific. 8-hydroxyquinoline (Hqn), N-ethylmorphine (NEM), and cobalt (II) tetrafluoroborate
hexahydrate ($Co(BF_4)_2$) were purchased from Sigma-Aldrich. HPLC graded water was purchased from Sigma-Aldrich. MilliQ water at 18 MΩ cm was used for all experiments.

2.2 Peptoid synthesis protocols

All peptoid synthesis was carried out on Rink amide resins. First, Rink amide resins (100 mg, 0.09 mmol) were first swelled in N,N-dimethylformamide (DMF) for 10 minutes. Afterward, the resins were

filtered, and the Fmoc groups were removed by adding 2 mL of 20% (v/v) 4-methylpiperidine/DMF solution. The mixture was then shaken at room temperature for 40 minutes. Subsequently, the resins were drained and washed with DMF using 5 washes of 1 mL each. Afterward, the deprotected resins underwent an acylation reaction (Scheme S1a) using 1.5 mL of 0.6 M bromoacetic acid and 0.3 mL of a 50/50 (v/v) N,N-diisopropylcarbodiimide (DIC)/DMF mixture. The reaction mixture was shaken for 10 minutes at room temperature, followed by washing with DMF (5 × 1 mL). Nucleophilic displacement of bromide with the submonomers (Scheme S1b) was achieved by adding 1.5 mL of a 0.6 M primary amine solution in N-methyl-2-pyrrolidone (NMP) and agitating for 10 minutes at room temperature. The solution was then filtered, and the resins were washed with DMF (5 × 1 mL). The acylation and displacement reactions with appropriate primary amines [such as 4-bromophenethylamine (Nbrpe), tert-butyl (2-aminoethyl)carbamate (Nae) or β-alanine tert-butyl ester (Nce)] were repeated until the desired target peptoid sequence was obtained.

To introduce 8-hydroxyquinoline (Hqn), the peptoid was mixed with 1.5 mL of 0.6 M bromoacetic acid and 0.3 mL of 50/50 (v/v) DIC/DMF for 10 min before removing the supernatant and washing with DMF (5 × 1 mL). Subsequently, 1.5 mL of 0.6 M of tris(2- aminoethyl)amine in NMP was added to the above resin, and the mixture was stirred overnight at

room temperature, filtered, and washed with DMF (5 × 1 mL). Furthermore, an acylation cycle was performed using 1.5 mL of 0.6 M bromoacetic acid and 0.6 mL of 50/50 (v/v) DIC/DMF. Nucleophilic displacement of bromide with the submonomers occurred by adding 1.5 mL of 0.6 M benzylamine solution in NMP, followed by agitating for 10 min at room temperature. The solution was filtered off, and the resins were washed with DMF (5 × 1 mL). One more acylation cycle was performed using 3 mL of 0.6 M bromoacetic acid and 0.6 mL of 50/50 (v/v) DIC/ DMF. Finally, 3 mL of 0.6 M Hqn in NMP and 200 mg K2CO3 were added to the above resin, and the mixture was stirred overnight at room temperature, filtered, and washed with DMF (5 × 1 mL).

2.3 Purification

The cleavage of peptoids from the resins was carried out by treating the bead resins with 3 mL of 95/5 (v/v) trifluoroacetic acid (TFA)/H_2O for 30 minutes with agitation. The solution was collected and the TFA solution was evaporated under reduced pressure at 36 ^{o}C. The crude peptoid product was dissolved in 80/20 (v/v) acetonitrile/ H_2O and purified by reverse-phase high-performance liquid chromatography (HPLC, Water 1525) set up with an XBridgeTM Prep C18 OBDTM column, 10 µm, 19 mm×100 mm, using a linear gradient of 45 – 55 % (for Nbrpe6Nce6Hqn2) or 50 – 70% (for the other peptoids) acetonitrile in water with 0.1% TFA.

Mass spectrometry characterization was conducted for purified peptoid.

2.4 Binding test of peptoid with metal

Used 95% TFA to dissolve the purified peptoid and left it for 10 minutes. Then, the peptoid TFA solution was dried by N_2 gas flow. Pure acetonitrile was added to make a 1 mM peptoid stock solution. Pure acetonitrile was used for blanking; the range of wavelengths was 190 – 850 nm. After blanking, 200 µL (or 400 µL) of the 1 mM peptoid stock solution was diluted in 800 µL (or 600 µL) of acetonitrile to attain a final concentration of 0.2 mM (or 0.4 mM). Each peptoid was titrated separately to obtain the absorbance spectrum of individual complexes by adding 1 µL of M^{2+} ($Zn(BF_4)_2$, $Co(BF_4)_2$, $Cu(BF_4)_2$) solution. The change in absorbance at specific wavelengths was extracted to determine the binding ratio between metal and peptoid. Quantitative analysis of the metal-peptoid binding efficiency was conducted.

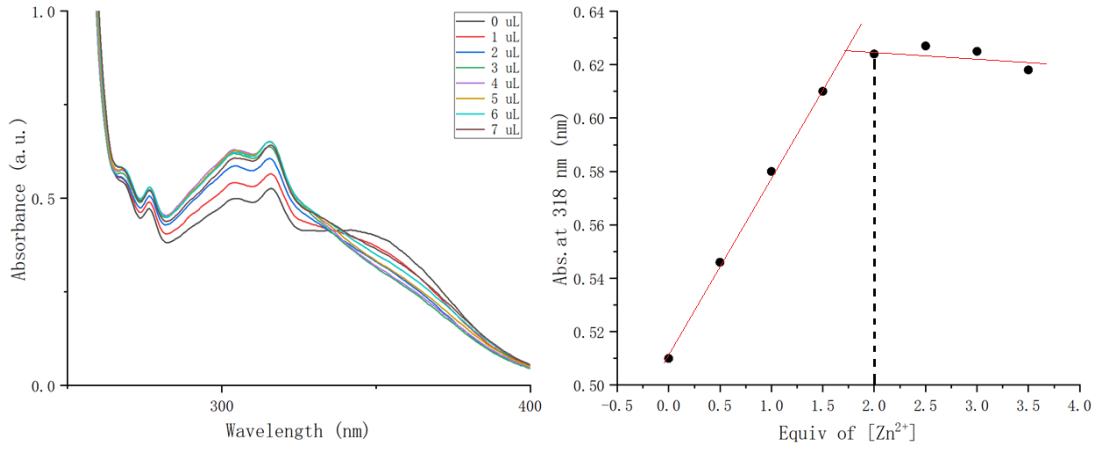

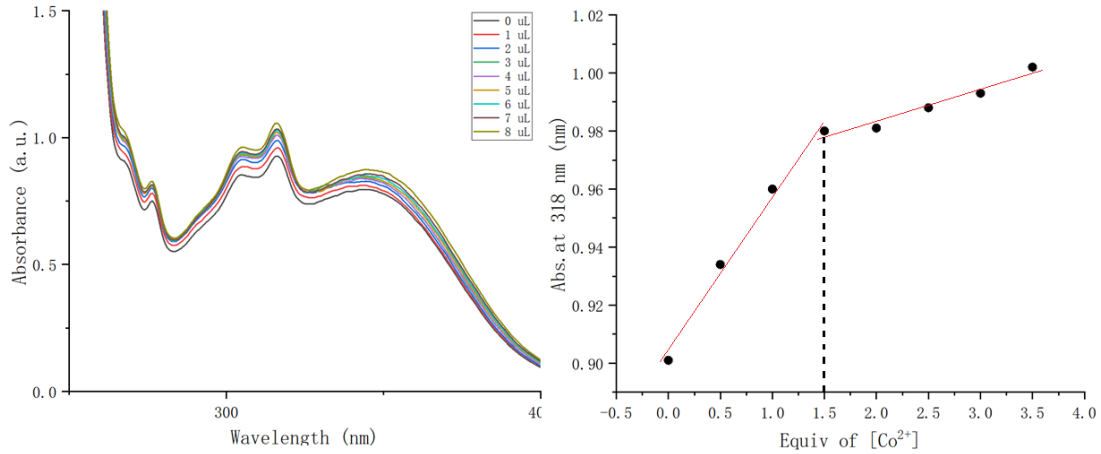

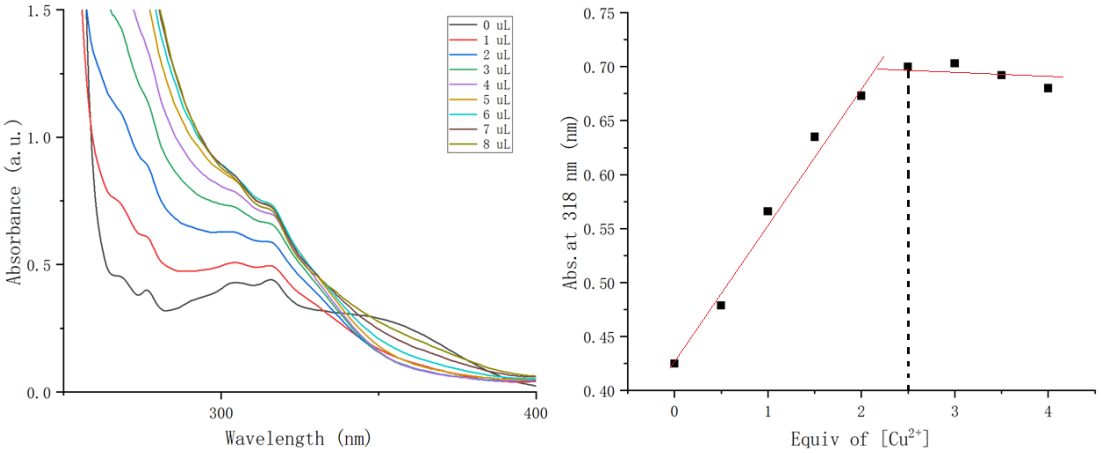

2.5 Metal binding and self-assembly of peptoids

Metal binding with peptoids

0.2 umol of peptoid is prepared in 1 ml centrifuge tube, add 95% TFA to dissolve it. Leave for 10 minutes. Then the peptoid TFA solution was dried by N_2 gas flow. Pure acetonitrile was added to dissolve all TFA treated peptoid. Added metal tetrafluoroborate acetonitrile solution and made sure the ratio of peptoid and metal cation is consistent with the results of binding test. Added pure acetonitrile to make the final volume 100 ul. Left for overnight.

Self-assembly of metal-bound peptoids

Added 100 ul of deionized H_2O into the centrifuge tube to make 1/1 (v/v) H_2O-acetonitrile metal-bound peptoid solution, added NaOH to adjust the pH to 7-8. Sonicated the solution to make it homogeneous. Made a small hole on the cap of centrifuge tube, put it in room temperature and let it volatilize. After around 3-5 days, a gel like solution can be observed. Added 100 uL deionized H_2O to make 1 mM stock solution.

2.6 Characterization

Atomic force microscopy (AFM)

AFM experiments were performed on the Bruker Icon using Scanasyst mode or Peakforce mode under room temperature. To prepare an AFM sample, 1 uL peptoid self-assembly solution was diluted with 19 uL deionized water and dropped onto a freshly peeled mica surface for 10 minutes. Used filter paper to blotte the solution on mica surface and then dried by N_2 gas flow.

Transmission electron microscopy (TEM)

TEM experiments were performed on the FEI Tecnai G2 F20 Supertwin TEM operating at an accelerating voltage of 200 keV. The peptoid sample was characterized under both bright field mode and STEM mode. To prepare a TEM sample, 1 uL peptoid self-assembly solution was diluted in 19 uL deionized water, and dropped onto a pure carbon 300 mesh copper grid for 10 minutes. Blotted the solution dry with filter

paper. For the negative staining, add 10 uL phosphotungstic acid (PTA) (wt 1%) onto the grid for 1-3 minutes. Blotted the extra PTA solution dry with filter paper. Then added 10 uL of deionized H_2O onto the grip to wash away the remaining PTA and blotted the deionized H_2O dry with filter paper. Finally, put the grid in fume hood to let it dry.

2.7 Catalytic activity assay for peptoid-based CA mimic

UV-vis measurements

As mentioned in 1.3.3, we can use p-nitrophenol acetate (p-NPA) assay to determine the catalytic activity of peptoid-based CA mimic. In detail, added 234 uL of 50 mM HEPES buffer (pH=7.4) into a 4 ml vial. Then 60 uL of 1 mM peptoid self-assembly stock solution was added into the vial as pre-mixed solution. Control groups used 60 uL of deionized H_2O or the metal salt solution instead. Left for overnight.

UV-vis measurement was conducted on Thermo Fisher nanodrop one using automated pathlength mode. Blanking with 60 uL of deionized H2O +234 uL of 50 mM HEPES buffer. UV-vis of pre-mixed solution was measured three times as uncatalyzed absorbance. Added 6 uL of 10 mM p-NPA acetonitrile solution and a stir bar into the vial to initial reaction. The final volume was 300 uL and the final concentrations of peptoid assemblies and p-NPA were both 200 uM. The absorbances were measured three times every 15 minutes for 2 hours.

Standard curve

To calculate the conversion rate of p-NPA to p-NP, the standard curve of the absorbance of p-NP as a function of concentration was needed. P-NP has the largest absorbance at 402 nm (Figure 2-1), so we choose to measure the absorbance at 402 nm. To prepare the standard curve, first is to prepare 40 mM p-NP in acetonitrile solution and 50 mM HEPES buffer first. Then 200 uM p-NP solution was prepared by diluting 40 mM p-NP with 50 mM HEPES buffer, followed by mixing the 200 uM p-NP solution with 50 mM HEPES buffer in a different ratio, forming a series concentration of p-NP solution 0, 40, 80, 120,160 and 200 uM. UV-vis absorbances were measured three times at 402 nm for each p-NP concentration. The standard curve is shown in Figure 2-2.

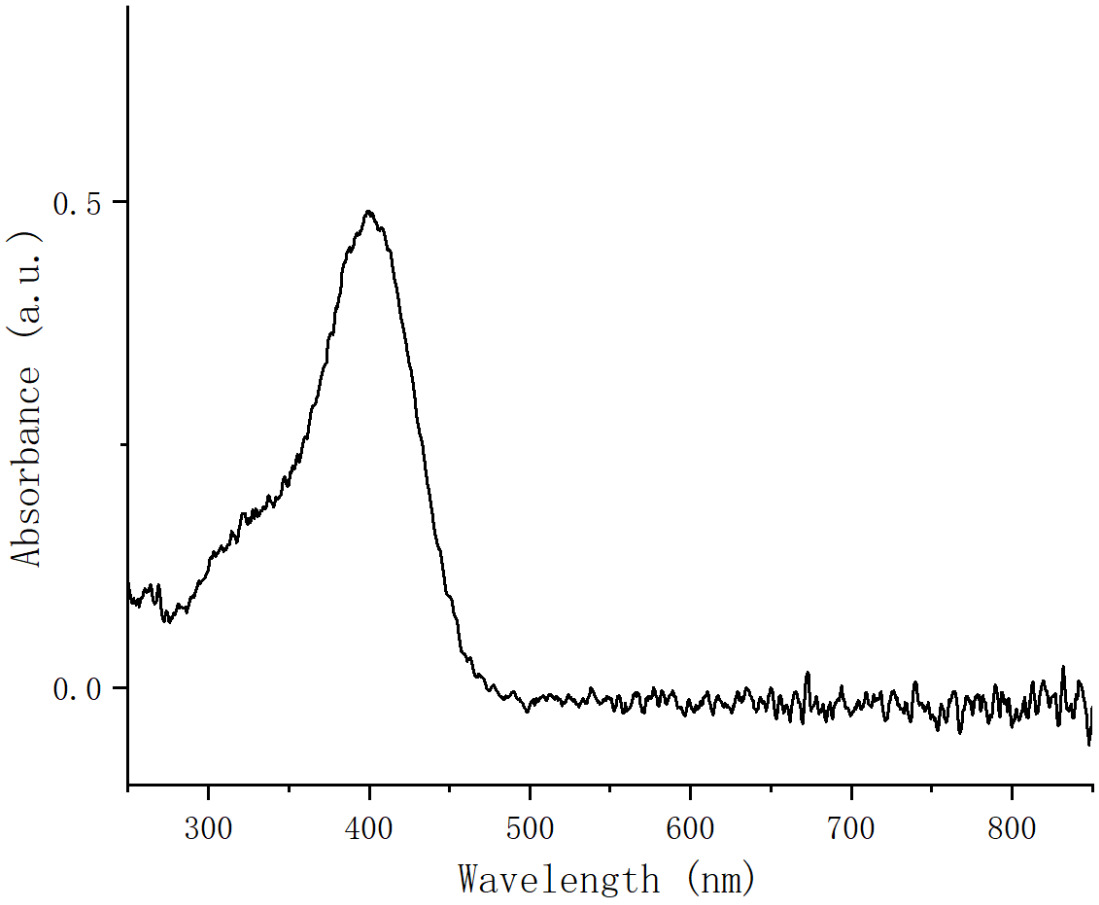

Figure 2-1 UV-vis spectrum of p-NP

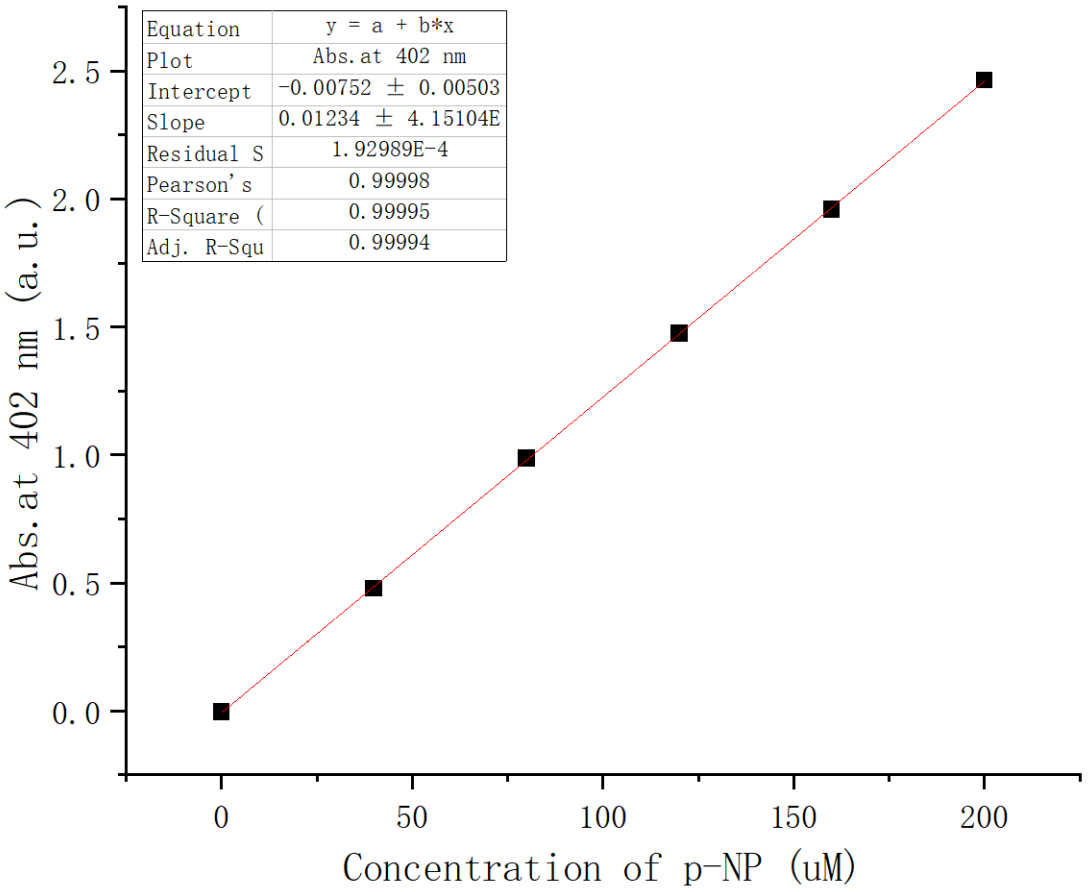

Figure 2-2 Standard curve

RESULTS AND DISCUSSION

3.1 Pep-1-M^{2+} self-assembly and characterization

As discussed previously, we aimed to develop a peptoid-based CA mimetic heterogeneous catalyst. We design a series of peptoids with hydrophobic domain, hydrophilic domain, and ligand domain. The chemistry of hydrophobic domain plays a leading role in controlling the morphology of peptoid assemblies. This domain contains six N-([2-(4-bromophenyl)ethyl]glycine) groups(Nbrpe), with π-π interactions between aromatic groups, the peptoid can form ordered structures like nanotubes or nanosheets by self-assembly.[14] The hydrophilic domain

contains zero, three, and six N-(2-aminoethyl)glycine) groups, respectively. We intend to explore the effect of different numbers of hydrophilic groups. The ligand domain is the most important one which contains an 8-hydroxyquinoline group that can coordinate transition metals with nitrogen and oxygen atoms to mimic the active site of CA. As discussed in 1.2, single molecule biomimetic catalyst is stable but difficult to recycle. We attached the single molecule CA mimic to the peptoid sequence, and peptoid can form ordered nanostructures by self-assembly or be attached to other substrates, which makes it much easier to separate or reuse.

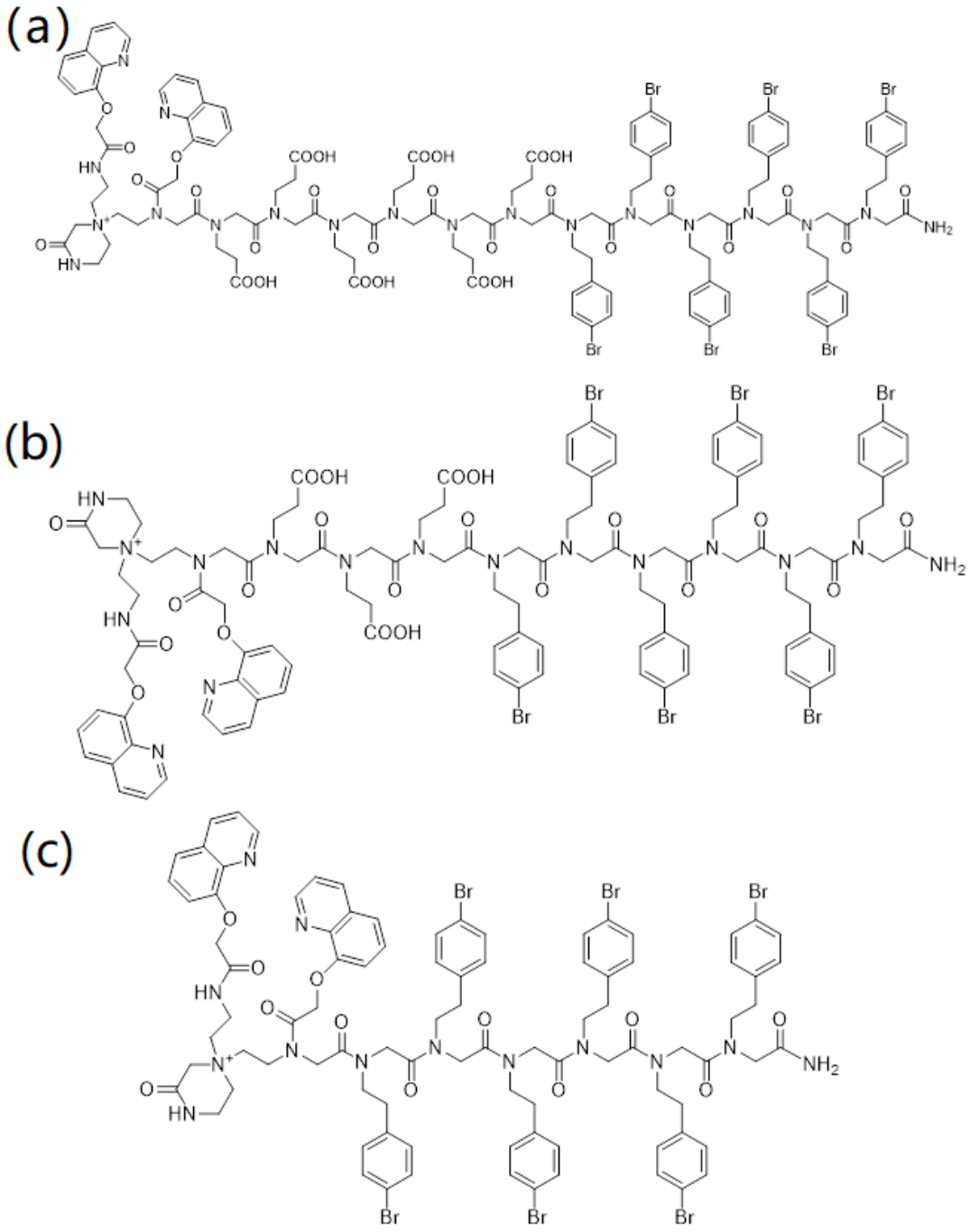

Figure 3-1 Structure of peptoids. (a) Pep-1: Nbrpe6Nae6Hqn2. (b) Pep-2: Nbrpe6Nae3Hqn2. (c) Pep-3: Nbrpe6Hqn2.

There are three steps to prepare peptoid assemblies. First step, the peptoid powder needs to be treated with TFA to make sure peptoids are not aggregated or self-assembled before the experiments. Prepare 0.2 umol of

peptoid powder in the 1ml centrifuge tube. Added 10 ul of 95% TFA to dissolve it, a reddish clear solution is obtained. Used N_2 gas flow to remove TFA, a sticky reddish remnant can be observed. Added some acetonitrile to dissolve it, then added metal tetrafluoroborate according to the ratio determined by binding test. Added more acetonitrile to 100 uL to make the concentration consistent. Left for overnight. Add 100 uL of deionized H_2O into the centrifuge tube to make H_2O-acetonitrile mixed solution (v/v = 1:1) and added NaOH to adjust pH to 7-8. Make a small hole in the cap and leave it at room temperature, self-assembly is triggered as acetonitrile evaporates. After 5-7 days, a translucent gel like solution can be observed. For pep-1-Co^{2+} and pep-1-Zn^{2+}, the solutions were homogeneous. For pep-1-Cu^{2+}, there was some precipitation in the solution. Added deionized H2O into the centrifuge tube to make final volume 200 uL, this ensured each sample had the same concentration. Each sample was characterized using AFM and TEM.

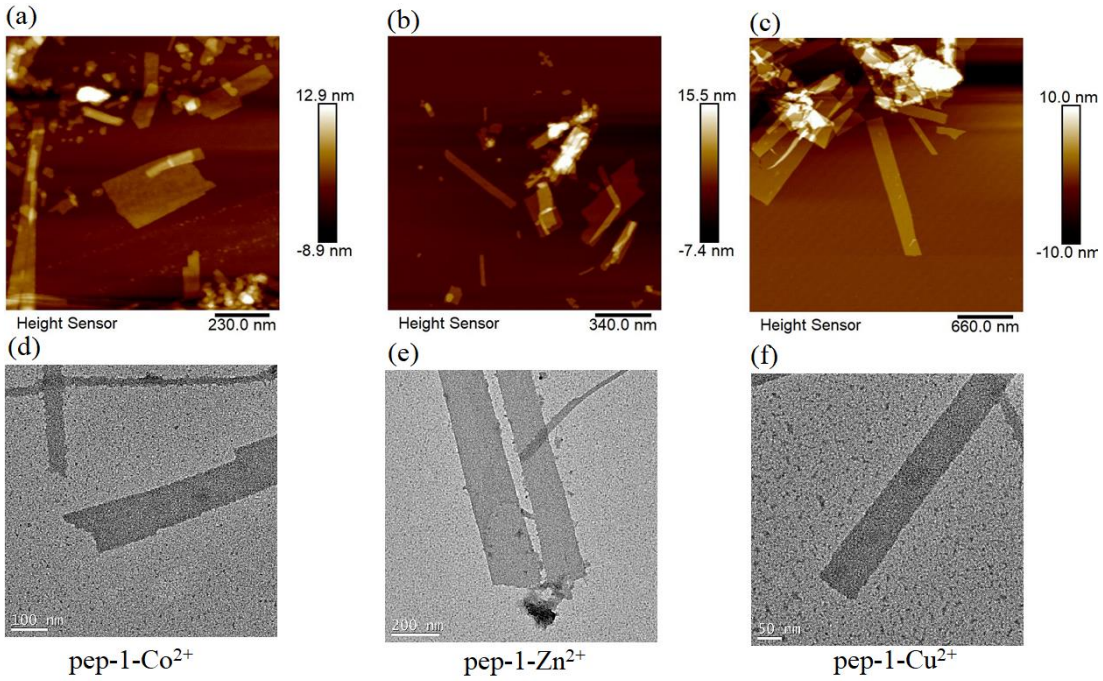

Figure 3-2 AFM and TEM images of pep-1-M^{2+} nanosheets. (a), (d) AFM and TEM images of pep-1-Co^{2+}. (b), (e) AFM and TEM images of pep-1-Zn^{2+}. (c), (f) AFM and TEM images of pep-1-Cu^{2+}

As we can see in Figure 3-2, all the samples formed nanosheets. Pep-1-Co^{2+} nanosheets were more finely divided, while some pep-1-Zn^{2+} and pep-1-Cu^{2+} nanosheets were aggregated together. Then the p-NPA assay was conducted to test the catalytic activities of these samples.

3.2 P-NPA hydrolysis test of Pep-1-M^{2+} nanosheets

P-NPA hydrolysis tests were conducted following the protocol in 2.7. As p-NPA was converted into p-NP, the solution gradually turned yellow. The absorbances were measured in 15- or 30-minute intervals.

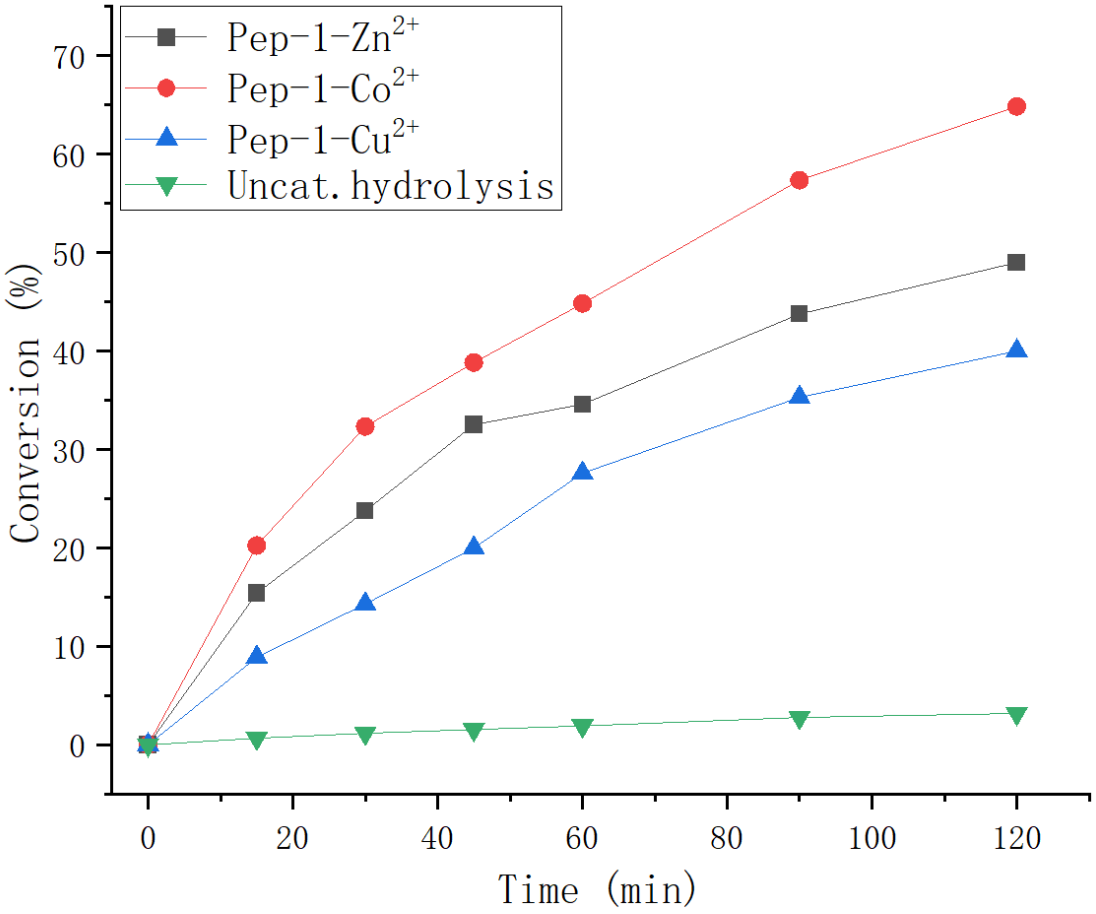

Figure 3-3 Hydrolysis profile of p-NPA hydrolysis catalyzed by Pep-1-M^{2+} nanosheets.

The p-NPA conversion rate vs. time is shown in Figure 3-3. Among these nanosheets, pep-1-Co^{2+} nanosheets had the best catalytic activity, pep-1-Zn^{2+} nanosheets were intermediate, while pep-1-Cu^{2+} nanosheets had relatively lower activity. Almost no hydrolysis occurred when there were no nanosheets present. The difference in activity between each type of nanosheet could have had several causes. First, the amount of metal cations bound to the peptoid might have influenced the activity. Referring to the binding test in Section 2.4, metal cations bind with the peptoid in different ratios: one equivalent of peptoid binds with 1.5, 2, and 2.5

equivalents of Co^{2+}, Zn^{2+}, and Cu^{2+}, respectively. However, the results of the hydrolysis were the opposite: the more equivalents of metal cations that bound with the peptoid, the lower the activity of the nanosheets was, suggesting that there must be other factors. Trinh et al. reported that the electronegativity of metal cations may affect their activity. The metal cation with the highest electronegativity should have the best activity. The electronegativities of these ions are: Zn^{2+} ($\chi = 1.65$) < Co^{2+} ($\chi = 1.88$) < Cu^{2+} ($\chi = 1.90$) [25]. This leads to another question: why does Cu^{2+}, despite having the highest electronegativity and binding ratio, have the lowest activity? The third factor could be the difference in the degree of dispersion of the nanosheets affected by metal cations.

As previously mentioned, after 5-7 days self-assembly, pep-1-Co^{2+} and pep-1-Zn^{2+} formed gel like homogenous solution, while pep-1-Cu^{2+} solution had some precipitation inside. This could be the aggregates of nanosheets or metal hydroxide precipitation. $Cu(OH)_2$ has the lowest Ksp, which is 2.20×10^{-20}, while Ksp of $Zn(OH)_2$ and $Co(OH)_2$ is 3.00×10^{-16} and 1.0×10^{-15}, respectively. That means Cu^{2+} precipitates more easily under alkaline condition. However, an alkaline condition is needed for self-assembly of this series of peptoid sequences. This could explain why there was precipitation observed in pep-1-Cu^{2+} solution. In addition, according to binding test, we added more equivalent of Cu2+ than Zn2+ and Co^{2+}, which also made Cu^{2+} easier to precipitate and made the

catalyst less efficient. This effect may also make nanosheets aggregate together and reduce the exposed area. All these factors could cause the lower activity of Cu^{2+} containing nanosheets.

3.3 Effect of hydrophilic domain length on peptoid-based CA mimic activity

To examine the effect of hydrophilic domain length on peptoid-based CA mimic, we prepared the self-assembly solution of pep-2 and pep-3 with the same ratio of Co^{2+} added since pep-1-Co^{2+} had the best activity. Unlike pep-1 which form homogenous solution, we found some precipitation in pep-2 and pep-3 sample. TEM and AFM were used to characterize the morphology of these samples.

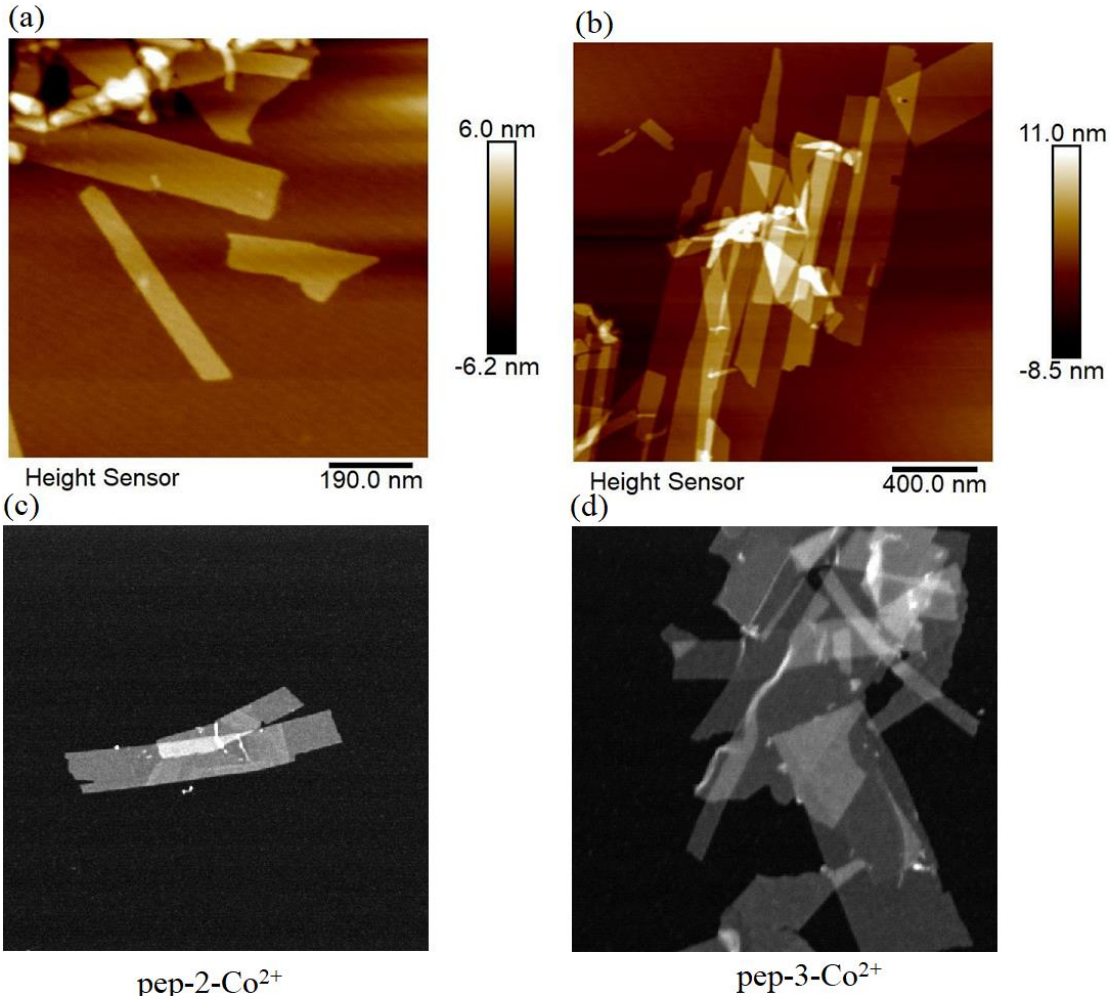

Figure 3-4 Effect of hydrophilic domain lengths on the morphology of nanosheets. (a)

As shown in Figure 3-4, nanosheets formed by both pep-2-Co^{2+} and pep-3-Co^{2+} had certain degrees of overlap, especially the pep-3-Co^{2+}. As mentioned previously, we observed precipitation in both sample solutions, but we only took the supernatant from both solutions to prepare the AFM and TEM samples. Therefore, we could not see aggregates of large particles in these images. But this indicated that the lengths of the hydrophilic domains would affect the self-assembly since the other conditions remain unchanged. p-NPA assay was conducted with the same

conditions as above to test the catalytic activities. The results are shown below.

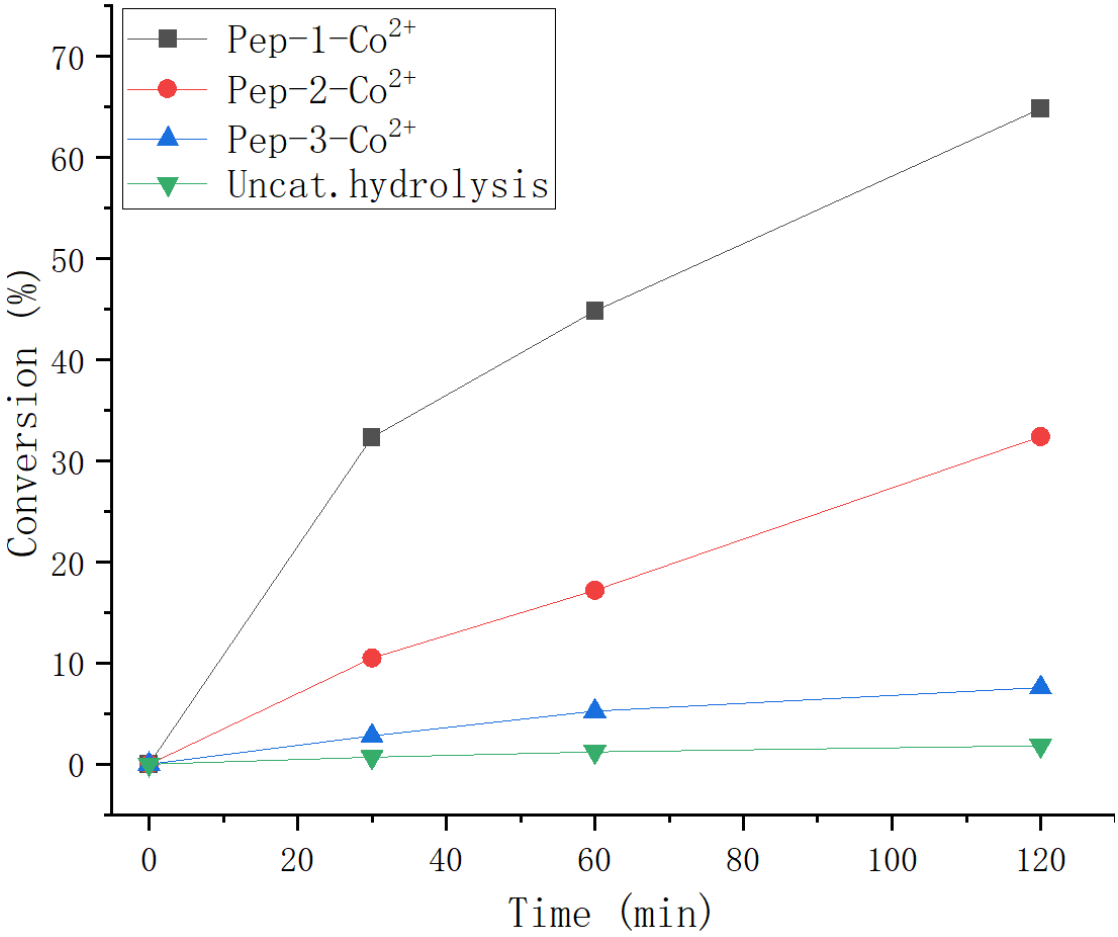

Figure 3-5 Hydrolysis profile of p-NPA hydrolysis catalyzed by Co^{2+} containing nanosheets formed by peptoids with different hydrophilic domain lengths.

The results showed that pep-1-Co^{2+}, with the longest hydrophilic domain, had the best activity, with a conversion rate of p-NPA of 64.8% after 120 minutes. Pep-2-Co^{2+} was the second-best, with a conversion rate of 32.4%, while pep-3-Co^{2+} had the worst activity, with just 7.6% conversion after 120 minutes, only slightly better than the uncatalyzed condition. One obvious reason was that the shortening of the hydrophilic domain made the assemblies easier to aggregate; even in the supernatant

of the samples, we could observe the overlap of nanosheets, which reduced the activities.

So far, we can draw a rough conclusion: differences in binding metals or hydrophilic domain lengths affect the self-assembly of peptoid nanosheets, most likely through different mechanisms. Different metal cations and varying amounts of them might cause different coordination patterns or supramolecular interactions, leading to precipitation and thus affecting self-assembly. Furthermore, different metal cations have different properties like electronegativity. Even if they do not affect the self-assembly, the activities are also very likely to differ.

Another problem arises at this time, we cannot determine which is responsible for the activity. Another set of controlled experiments is needed.

3.4 Controlled experiments of peptoid-metal complex

In this experiment, we prepared four control groups: (I) Pep-1-Co^{2+} nanosheets; (II) Pep-1 nanosheets (without metal); (III) $Co(BF_4)_2$ solution; (IV) deionized H_2O, to ensure that it was the metal-containing peptoid nanosheet that exhibited the activity. (II) and (III) used the same amount and ratio of peptoid or Co^{2+} as in previous experiments. Other conditions were also the same. The results are shown below.

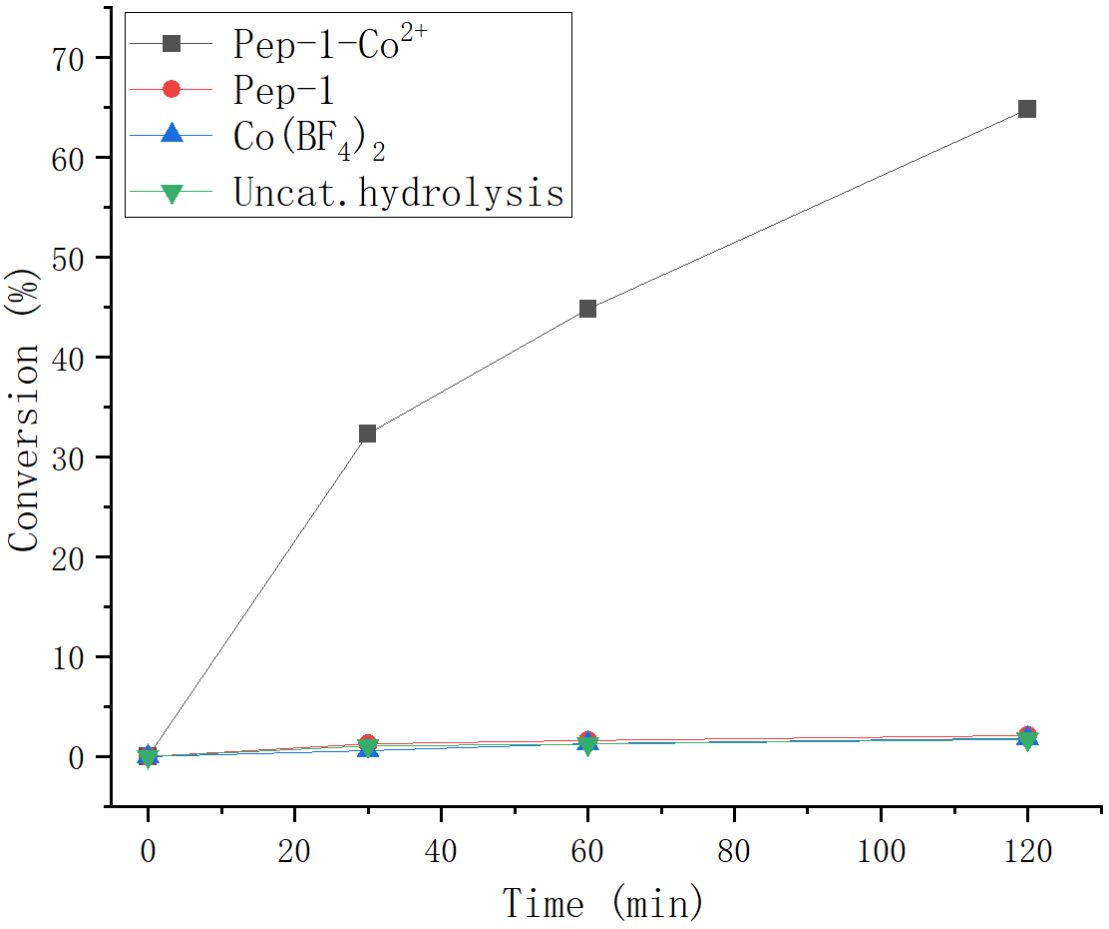

Figure 3-6 Hydrolysis profile of different control groups.

The results showed that peptoid only showed activity when bound to metal cations. If there are only metal cations or peptoids present, the hydrolysis progresses as slow as uncatalyzed condition.

3.5 Effect of self-assembly state on peptoid-based CA mimic activity

According to the above experiments, we still do not know if the self-assembly state affects the activity. For example, if the peptoid only binds

with metal but does not form nanosheets, or if metal cations are added after the nanosheets have formed, would they still exhibit activity? Thus, we did another set of controlled experiments. We prepared the following control groups: (I) Pep-1-Co^{2+} complex, this sample was prepared by evaporating the acetonitrile in fume hood after peptoid-metal binding, then 200 uL of deionized H_2O was added to make the concentration consistent. (II) Pep-1-Cu^{2+} complex, this sample was prepared with same protocol as above. (III) Pep-1 nanosheets + Co^{2+}, this sample was prepared by adding $Co(BF_4)_2$ water solution into the assembled pep-1 nanosheets, the ratio of peptoid and metal remained consistent. (IV) Pep-1-Co^{2+} nanosheets, the same sample as in 3.1. (V) Pep-1-Cu^{2+} nanosheets, the same sample as in 3.1. The result of the hydrolysis test is shown below.

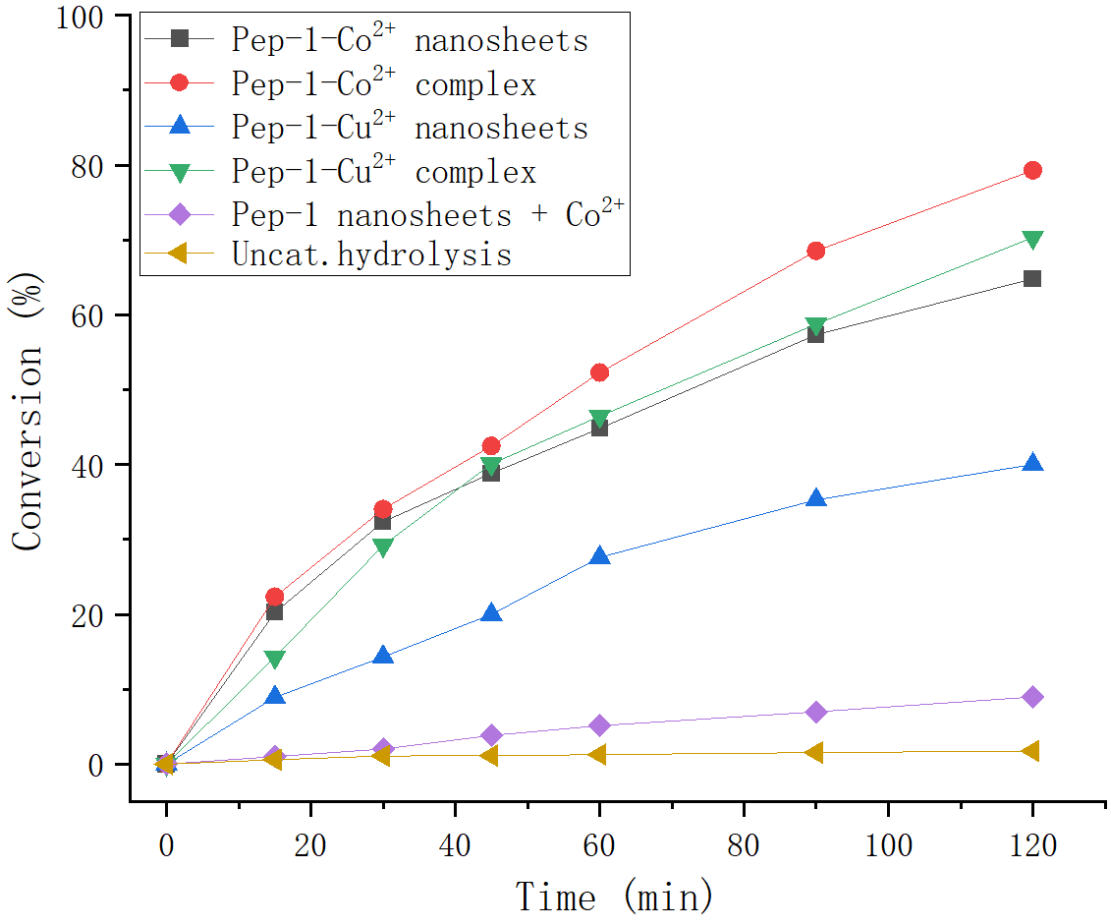

Figure 3-7 Hydrolysis test to examine the effect of self-assembly state.

This result provided us with a lot of information and confirmed some of the above hypotheses. First, increases in the activities of the pep-1-Co^{2+} and pep-1-Cu^{2+} complexes compared to their nanosheets were observed, which indicated that part of the activity was lost after the nanosheets were formed from peptoid-metal complex, which was reasonable. Based on what we discussed so far, when there was precipitation observed in self-assembly solution, that sample would most likely have lower activity than the homogeneous one. As we can see in this Figure 3-7, pep-1-Cu^{2+} complex has much better activity than pep-1-Cu^{2+} nanosheets. Previous

results indicated that large amounts of precipitation formed during self-assembly of pep-1-Cu^{2+} complex, and the activity reduced dramatically due to the reduced exposed area of nanosheets. For pep-1-Co^{2+} complex, which formed homogeneous gel like solution after self-assembly, its activity also decreased. This may be because pep-1-Co^{2+} complex had more effective collision opportunities with the substrate molecules p-NPA when it existed in solution as single molecule. We also observed that sample (III) had very low activity and there are two possible factors. First, we used $Co(BF_4)_2$ water solution instead of acetonitrile solution because the main solvent of the assembled solution is water, the binding may not be efficient as in acetonitrile. Second, metal cations could be difficult to bind with the ligands when nanosheets were already formed due to steric hindrance.

DISCUSSION

The above results show that all the metal-bound peptoid nanosheets exhibit hydrolytic activity of p-NPA, and many factors affect their ac activities such as metal cation, hydrophilic domain length, and self-assembly state. We got the best activity when pep-1 bound with Co^{2+} and only formed complex. However, the influence due to the length of the hydrophilic group is not very clear. Although we observed the formation of precipitates and partial overlap of nanosheets, its activity decreased far

beyond our expectations. We hypothesize that changes in the length of the hydrophilic group may also affect the binding of metal cations and ligands. Additional experiments are needed to prove this hypothesis.

REFERENCES

(1) Effendi, S. S. W.; Ng, I-Son. The Prospective and Potential of Carbonic Anhydrase for Carbon Dioxide Sequestration: A Critical Review. Process Biochemistry 2019, 87, 55–65. https://doi.org/10.1016/j.procbio.2019.08.018.

(2) Fuglestvedt, J.; Berntsen, T.; Myhre, G.; Rypdal, K.; Skeie, R. B. Climate Forcing from the Transport Sectors. Proceedings of the National Academy of Sciences 2008, 105 (2), 454–458. https://doi.org/10.1073/pnas.0702958104.

(3) Verma, M.; Bhaduri, G. A.; Phani Kumar, V. S.; Deshpande, P. A. Biomimetic Catalysis of CO2 Hydration: A Materials Perspective. Industrial & Engineering Chemistry Research 2021, 60 (13), 4777–4793. https://doi.org/acs.chemmater.1c00243/acs.iecr.0c06203.

(4) Kammerer, S.; Borho, I.; Jung, J.; Schmidt, M. S. Review: CO2 Capturing Methods of the Last Two Decades. 2022. https://doi.org/10.1007/s13762-022-04680-0.

(5) Lindskog, S. Structure and Mechanism of Carbonic Anhydrase. Pharmacology & Therapeutics 1997, 74 (1), 1–20. https://doi.org/10.1016/s0163-7258(96)00198-2.

(6) MacDowell, N.; Florin, N.; Buchard, A.; Hallett, J.; Galindo, A.; Jackson, G.; Adjiman, C. S.; Williams, C. K.; Shah, N.; Fennell, P. An Overview of CO2 Capture Technologies. Energy & Environmental Science 2010, 3 (11), 1645. https://doi.org/10.1039/c004106h.

(7) Supuran, C. T. Structure and Function of Carbonic Anhydrases. The Biochemical Journal 2016, 473 (14), 2023–2032. https://doi.org/10.1042/BCJ20160115.

(8) Seung Hwan Lee; Seung Woo Park; Soon Kwan Jeong; Kyoung Jae Lim; Si Hyeock Lee; Trachtenberg, M. C. On Carbon Dioxide Storage Based on Biomineralization Strategies. Micron 2010, 41 (4), 273–282. https://doi.org/10.1016/j.micron.2009.11.012.

(9) Vinoba, M.; Bhagiyalakshmi, M.; Jeong, S. K.; Yoon, Y. I.; Nam, S. C. Immobilization of Carbonic Anhydrase on Spherical SBA-15 for Hydration and Sequestration of CO2. Colloids and Surfaces B: Biointerfaces 2012, 90, 91–96. https://doi.org/10.1016/j.colsurfb.2011.10.001.

(10) Zuckermann, R. N. Peptoid Origins. Biopolymers 2010, 96 (5), 545–555. https://doi.org/10.1002/bip.21573.

(11) Gamba, I. Biomimetic Approach to CO2 Reduction. Bioinorganic Chemistry and Applications 2018, 2018, 1–14. https://doi.org/10.1155/2018/2379141.

(12) Zhang, X.; van Eldik, R. A Functional Model for Carbonic Anhydrase: Thermodynamic and Kinetic Study of a Tetraazacyclododecane Complex of Zinc(II). Inorganic Chemistry 1995, 34 (22), 5606–5614. https://doi.org/10.1021/ic00126a034.

(13) Floyd, W. C.; Baker, S. E.; Valdez, C. A.; Stolaroff, J. K.; Bearinger, J. P.; Satcher, J. H.; Aines, R. D. Evaluation of a Carbonic Anhydrase Mimic for Industrial Carbon Capture. Environmental Science & Technology 2013, 47 (17), 10049–10055. https://doi.org/10.1021/es401336f.

(14) Cai, B.; Li, Z.; Chen, C.-L. Programming Amphiphilic Peptoid Oligomers for Hierarchical Assembly and Inorganic Crystallization. Accounts of Chemical Research 2020, 54 (1), 81–91. https://doi.org/10.1021/acs.accounts.0c00533.

(15) Sakshi Yadav Schmid; Ma, X.; Hammons, J. A.; Mergelsberg, S. T.; Harris, B. S.; Ferron, T.; Yang, W.; Zhou, W.; Zheng, R.; Zhang, S.; Benjamin Adam Legg; Anthony Van Buuren; Baer, M. D.; Chen, C.-L.; Tao, J.; De, J. J. Influence of Peptoid Sequence on the Mechanisms and Kinetics of 2D Assembly. ACS Nano 2024. https://doi.org/10.1021/acsnano.3c10810.

(16) Zhao, M.; Zhang, S.; Zheng, R.; Alamdari, S.; Mundy, C. J.; Pfaendtner, J.; Pozzo, L. D.; Chen, C.-L.; De, J. J.; Ferguson, A. L. Computational and Experimental Determination of the Properties, Structure, and Stability of Peptoid Nanosheets and Nanotubes. Biomacromolecules 2023, 24 (6), 2618–2632. https://doi.org/10.1021/acs.biomac.3c00107.

(17) Zheng, R.; Zhao, M.; Du, J. S.; Tarunya Rao Sudarshan; Zhou, Y.; Paravastu, A. K.; De, J. J.; Ferguson, A. L.; Chen, C.-L. Assembly of Short Amphiphilic Peptoids into Nanohelices with Controllable Supramolecular Chirality. Nature communications 2024, 15 (1). https://doi.org/10.1038/s41467-024-46839-y.

(18) Zhang, S.; Hettige, J. J.; Li, Y.; Jian, T.; Yang, W.; Yao, Y.-C.; Zheng, R.; Lin, Z.; Tao, J.; De, J. J.; Baer, M.; Noy, A.; Chen, C.-L. Co-Assembly of Carbon Nanotube Porins into Biomimetic Peptoid Membranes. Small 2023, 19 (21). https://doi.org/10.1002/smll.202206810.

(19) Kim, J. H.; Kim, S. C.; Kline, M. A.; Grzincic, E. M.; Tresca, B. W.; Cardiel, J.; Karbaschi, M.; Dehigaspitiya, D. C.; Chen, Y.; Udumula, V.; Jian, T.; Murray, D. J.; Yun, L.; Connolly, M. D.; Liu, J.; Ren, G.; Chen, C.-L.; Kirshenbaum, K.; Abate, A. R.; Zuckermann, R. N. Discovery of Stable and Selective Antibody Mimetics from Combinatorial Libraries of Polyvalent, Loop-Functionalized Peptoid

Nanosheets. ACS Nano 2019, 14 (1), 185–195. https://doi.org/10.1021/acsnano.9b07498.

(20) Yang, W.; Yin, Q.; Chen, C.-L. Designing Sequence-Defined Peptoids for Biomimetic Control over Inorganic Crystallization. 2021, 33 (9), 3047–3065. https://doi.org/10.1021/acs.chemmater.1c00243.

(21) Wilbur, K. M.; Anderson, N. G. ELECTROMETRIC and COLORIMETRIC DETERMINATION of CARBONIC ANHYDRASE. Journal of Biological Chemistry 1948, 176 (1), 147–154. https://doi.org/10.1016/S0021-9258(18)51011-5.

(22) Verpoorte, J. A.; Mehta, S.; Edsall, J. T. Esterase Activities of Human Carbonic Anhydrases B and C. Journal of Biological Chemistry 1967, 242 (18), 4221–4229. https://doi.org/10.1016/s0021-9258(18)95800-x.

(23) Bond, G. M.; Stringer, J.; Brandvold, D. K.; Simsek, F. A.; Medina, M.-G.; Egeland, G. Development of Integrated System for Biomimetic CO2 Sequestration Using the Enzyme Carbonic Anhydrase. Energy & Fuels 2001, 15 (2), 309–316. https://doi.org/10.1021/ef000246p.

(24) Shank, R. P.; McComsey, D. F.; Smith-Swintosky, V. L.; Maryanoff, B. E. Examination of Two Independent Kinetic Assays for Determining the Inhibition of Carbonic Anhydrases I and II: Structure?Activity Comparison of Sulfamates and Sulfamides.

Chemical biology & drug design 2006, 68 (2), 113–119. https://doi.org/10.1111/j.1747-0285.2006.00423.x.

(25) Kim, T.; Jian, T.; Jin, B.; Nguyen, D.-T.; Zuckermann, R. N.; Chen, C.-L. Designed Metal-Containing Peptoid Membranes as Enzyme Mimetics for Catalytic Organophosphate Degradation. ACS Applied Materials & Interfaces 2023, 15 (44), 51191–51203. https://doi.org/10.1021/acsami.3c11816.